Patient-specific tissue engineered vascular graft for aortic arch reconstruction

(R) Check for updates

Hidenori Hayashi, MD,[a] Jacqueline Contento, BSE,[b] Hiroshi Matsushita, MD,[a] Paige Mass, MS,[b]
Vincent Cleveland, MS,[b] Seda Aslan, MS,[c] Amartya Dave, BS,[a] Raquel dos Santos,[a] Angie Zhu,[a]
Emmett Reid,[a] Tatsuya Watanabe, MD, PhD,[a] Nora Lee, MPAP, PA-C,[a] Tyler Dunn, BS,[a] Umar Siddiqi,[a]
Katherine Nurminsky, BS,[a] Vivian Nguyen, BA,[d] Keigo Kawaji, PhD,[d] Joey Huddle, MS,[e]
Luka Pocivavsek, MD, PhD,[f] Jed Johnson, PhD,[e] Mark Fuge, PhD,[g] Yue-Hin Loke, MD,[b]
Axel Krieger, PhD,[c] Laura Olivieri, MD,[h] and Narutoshi Hibino, MD, PhD[a,i]

ABSTRACT

Objective(s): The complexity of aortic arch reconstruction due to diverse 3-dimensional geometrical abnormalities is a major challenge. This study introduces 3-dimensional printed tissue-engineered vascular grafts, which can fit patient-specific dimensions, optimize hemodynamics, exhibit antithrombotic and anti-infective properties, and accommodate growth.

Methods: We procured cardiac magnetic resonance imaging with 4-dimensional flow for native porcine anatomy (n = 10), from which we designed tissue-engineered vascular grafts for the distal aortic arch, 4 weeks before surgery. An optimal shape of the curved vascular graft was designed using computer-aided design informed by computational fluid dynamics analysis. Grafts were manufactured and implanted into the distal aortic arch of porcine models, and postoperative cardiac magnetic resonance imaging data were collected. Pre- and postimplant hemodynamic data and histology were analyzed.

Results: Postoperative magnetic resonance imaging of all pigs with 1:1 ratio of polycaprolactone and poly-L-lactide-co-ε-caprolactone demonstrated no specific dilatation or stenosis of the graft, revealing a positive growth trend in the graft area from the day after surgery to 3 months later, with maintaining a similar shape. The peak wall shear stress of the polycaprolactone/poly-L-lactide-co-ε-caprolactone graft portion did not change significantly between the day after surgery and 3 months later. Immunohistochemistry showed endothelization and smooth muscle layer formation without calcification of the polycaprolactone/poly-L-lactide-co-ε-caprolactone graft.

Conclusions: Our patient-specific polycaprolactone/poly-L-lactide-co-ε-caprolactone tissue-engineered vascular grafts demonstrated optimal anatomical fit maintaining ideal hemodynamics and neotissue formation in a porcine model. This study provides a proof of concept of patient-specific tissue-engineered vascular grafts for aortic arch reconstruction. (JTCVS Open 2024;18:209-20)
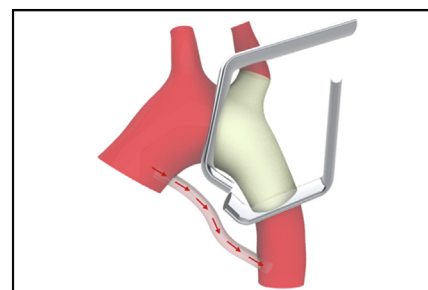
Patient-specific aortic tissue engineered vascular grafts implanted in porcine.

CENTRAL MESSAGE

Our patient-specific 3-dimensional tissue-engineered vascular grafts accommodated growth while maintaining ideal flow dynamics and morphology when implanted into the aortic arch of porcine subjects.

PERSPECTIVE

Patient-specific 3-dimensional tissue-engineered vascular grafts were successfully implanted in the aortic arch. In aortic surgery for patients with congenital heart disease, the use of patient-specific, growth-enabling, tissue-engineered vascular grafts have the potential to improve surgical outcomes and reduce the number of procedures required in a patient's lifetime.

Congenital heart disease (CHD) affects approximately 1% of live births worldwide and often requires complex vascular reconstruction.[1] Although surgical techniques and survival rates have improved, the overall risk of premature death for patients with complex heart disease remains elevated.[2,3] Therefore, innovative solutions are urgently needed to improve the long-term survival and quality of life for patients with CHD, including those with complex vascular anomalies.

Traditional surgical methods using homografts and synthetic patches have limitations, including material failure and lack of growth accommodation.[4] As a result, children with congenital heart defects often undergo multiple high-risk heart surgeries to replace grafts, posing greater risk of infection, longer hospital stays, and even death.[5,6] Undergoing multiple cardiothoracic operations and exposure to multiple episodes of cardiopulmonary bypass has also been associated with neurologic deficits.[7]

In recent years, patient-specific, 3-dimensional (3D)-printed, tissue-engineered vascular grafts (TEVGs) have emerged as a promising alternative. Studies have demonstrated the feasibility and potential efficacy of using 3D TEVGs for complex vascular reconstruction in CHD.[8] Whereas long-term results of using homografts and synthetic patches for Norwood procedures have shown risk of thrombosis and aneurysm formation, 3D TEVGs have shown to maintain excellent hemodynamic performance and accommodate growth over time.[9] In addition, in diseases that require aortic arch repair like aortic coarctation, interrupted aortic arch, and hypoplastic aortic arch, the implantation of TEVG may be an ideal alternative.

Our team has developed patient-specific, 3D TEVGs through magnetic resonance imaging (MRI), image segmentation, computer aided design (CAD) guided by computational fluid dynamics (CFD), and 3D-printed mold-based electrospinning (Figure 1).[10,11] CFD simulation explores multiple surgical solutions while predicting postoperative hemodynamics like wall shear stress (WSS), flow splits, and energy loss.[12,13] Our previous work in silico reveals that customized grafts, optimized using CFD, outperform standard grafts in terms of hemodynamic parameters,[10] demonstrating the potential to improve surgical CHD outcomes.

In vivo studies also validate the feasibility of patient-specific 3D TEVGs to promote cellular proliferation and maturation with potential for growth and anatomic reconstruction. For example, customized 3D TEVGs in preclinical studies of sheep models demonstrated decreased thrombogenicity and pressure gradients, as well as similar mechanical and histological properties as native tissue.[14] We also revealed similar outcomes of patient-specific 3D TEVGs in a porcine model, including comparable WSS, pressure drops, and pulmonary blood flow balance to the native vessel.[15] Lastly, ideal hemodynamics have been shown to be maintained after 10 weeks as the TEVG grows.[16]

Although many 3D TEVGs have shown good biocompatibility, the graft must also have the mechanical strength to withstand the harsh environment of the aorta. There have been no previous studies that have designed ideal hemodynamic shapes for 3D TEVGs using CFD and studied the changes over time when implanted into the aortic arch of a large animal. In this study, we hypothesized that maintaining the ideal shape is crucial for high-pressure systems and assessed the effectiveness of 3D TEVGs when implanted into the aortic arch.

MATERIALS AND METHODS
MRI Acquisition, 3D Model Design, and Scaffold Fabrication

The Institutional Animal Care and Use Committee (#72605; approved October 24, 2019) approved all procedures conducted at the University of Chicago Medical Center. The animals received humane care in accordance with the Guide for the Care and Use of Laboratory Animals (Facility RRID:SCR_021806). At approximately 1 month before implantation surgery, 14-week-old porcine subjects weighing roughly 30 kg underwent MRI using a 32-channel torso array on a 3.0 T magnet (Philips Ingenia). The MRI acquisition involved a 4-dimensional (4D) time-resolved magnetic resonance angiography with keyhole sampling scheme over the cardiothoracic region using a sagittal view, with acquisition parameters stated in previous work.[17] Magnetic resonance angiography image segmentation, stereolithography file export methods, CFD simulation and optimization (Figure 2), and graft design methods using CAD have been described in previous work.[17]

The porcine subjects were separated into 2 groups based on the type of material used for scaffold fabrication and compared. One group (n = 8) received grafts made of a biodegradable nanofiber material made of polycaprolactone (PCL) and poly-L-lactide-co-ε-caprolactone (PLCL) in a 1:1 ratio, and the other group (n = 2) received grafts made of a biodegradable nanofiber material made of polyglycolic acid (PGA) and PLCL in a 1:1 ratio. Both grafts were fabricated by wrapping them around a steel mandrel (Nanofiber Solutions). The detailed preparation and sterilization of the grafts are described in detail in previous work.[17]
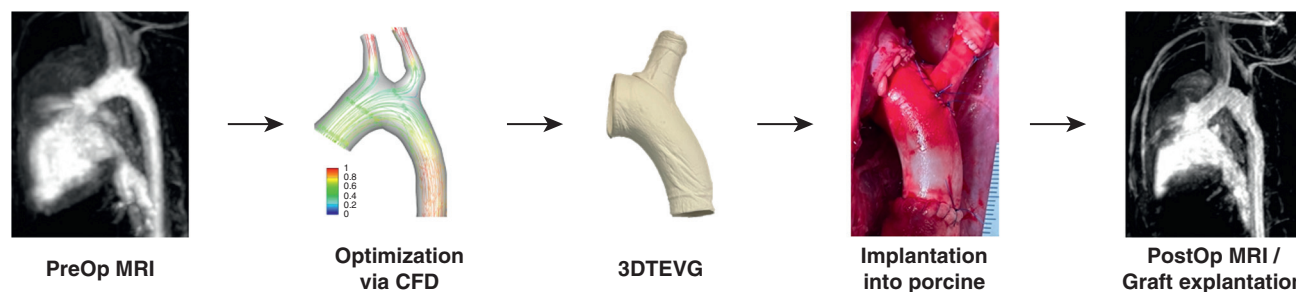
FIGURE 1. The workflow for this study. First, each porcine underwent preoperative (*preop*) magnetic resonance imaging (*MRI*). Then, customized grafts designed by computational fluid dynamics (*CFD*) optimization are 3-dimensional (*3D*) printed by electrospinning. The grafts were inserted via thoracotomy. After each follow-up period, each porcine subject underwent postoperative (*postop*) MRI, and the grafts were explanted. *TEVG*, Tissue-engineered vascular graft.

In Vivo Graft Implantation

One month after preoperative 4D flow MRI imaging, each porcine model was implanted with a 3D TEVG of its own shape and size using the TEVG manufacturing workflow detailed in Figure 1. Two animals received PGA/PLCL grafts, and 8 animals received PCL/PLCL grafts. Among the 8 animals that received PCL/PLCL grafts, 4 were assigned to the 1-day follow-up group, 2 to the 1-month follow-up group, and 2 to the 3-month follow-up group.

Grafts were implanted via left thoracotomy under general anesthesia and partial bypass of the ascending and descending aorta after the removal of one rib to increase exposure. Specifically, 3D TEVGs were implanted following the removal of the distal aortic arch to the proximal descending aorta, including the bifurcation of the left subclavian artery (Figure E1). All pigs survived surgery and were extubated in the operating room. Grafts were explanted on the last day of the follow-up period.

Data Analysis

Each pig model underwent postoperative 4D flow MRI imaging before graft removal on the last day of the follow-up period to confirm implantation of the graft, assess hemodynamics within the vessel, and analyze graft growth. In addition, the shape of the aorta with expected growth was compared with the actual graft. Hemodynamic factors of WSS, energy loss, right-handed helicity, and vorticity were measured as detailed in previous studies.[18]

To analyze the geometric differences between each time course, we determined the shape index of each 3D mesh utilizing MATLAB (MathWorks). Shape index is a continuous descriptor of shape between -1 and 1 that characterizes concave (-1), spherical (1), flat (0), ideal cylinder (0.5), and any in-between geometries through the calculation of curvature tensor values.[19] Shape index values were then overlaid as a heatmap on top of the 3D mesh for each subject at each time point to qualitatively assess geometrical change in the aortic wall over time. Finally, the mean and
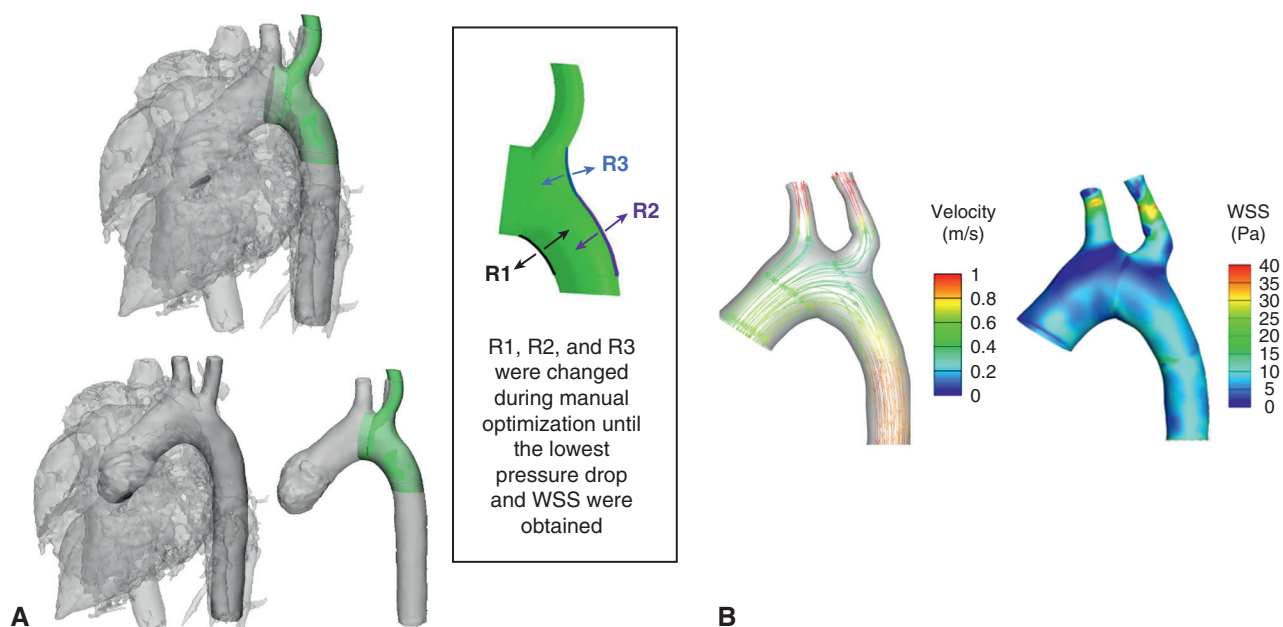
FIGURE 2. Three-dimensional (*3D*) tissue-engineered vascular graft optimization using computer-aided design and computational fluid dynamics. A, The 3D model of the surrounding heart and vasculature anatomy overlaid with the new graft design to test anatomical fit. B, The design with the best performance was determined based on the optimization of blood flow velocity and reduction of wall shear stress (*WSS*). *Blue* indicates the minimum value and *red* indicates the maximum value.
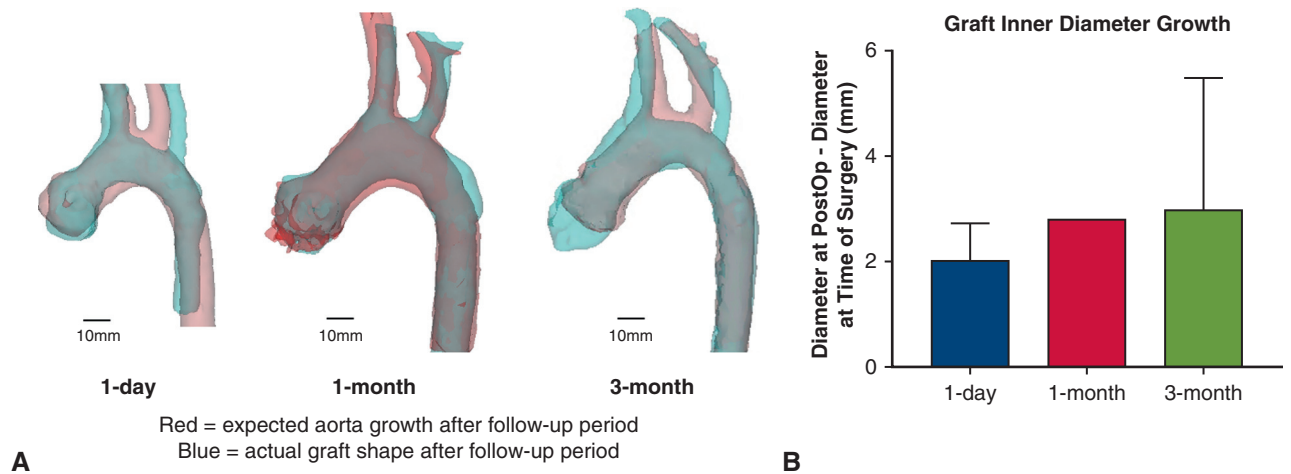
FIGURE 3. Graft growth assessment. A, Overlay of pre- and postoperative (*postop*) magnetic resonance imaging (*MRI*) images. *Red* shows expected aorta growth after the follow-up period and *green* shows actual graft shape after the follow-up period. B, Comparison of mean graft inner diameter of each group using MRI images.

variance of the shape index for each mesh was calculated, allowing for quantitative intra-subject comparisons using percent difference.

The same histological, mechanical, and statistical analysis methods were used from previous work; however, CD 68 (Abcam, ab955) and CD 206 (Novus Biologicals, NBP1-90020) were added for immunofluorescence testing.[16,17]

RESULTS

Porcine Growth

All 10 pigs survived surgical implantation; however, those with PGA/PLCL grafts died due to graft rupture on postoperative days 2 and 5, respectively. All 8 pigs with PCL/PLCL grafts survived their respective scheduled follow-up periods.

The surviving porcine models, which belong to the White Yorkshire crossed with Landrace breed, underwent preoperative MRI at age 10 weeks, surgery at 14 weeks, and postoperative MRI on the day after surgery (n = 4), at 18 weeks postoperative (n = 2), or 26 weeks postoperative (n = 2). The average weight of the pigs was 30.04 ± 0.95 kg at the preoperative MRI, 39.09 ± 3.07 kg at the time of surgery, 47.2 ± 2.83 kg at 18 weeks, and 78.5 ± 0 kg at 26 weeks (Figure E2). Thus, this weight trend was consistent with the general pig growth curve we used for estimation.[15]

Graft Shape Over Time

Postoperative MRI demonstrated no specific dilatation or stenosis of the graft. Graft inner diameter growth was measured as the difference between the inner diameter at the end of follow-up and the inner diameter at surgery.
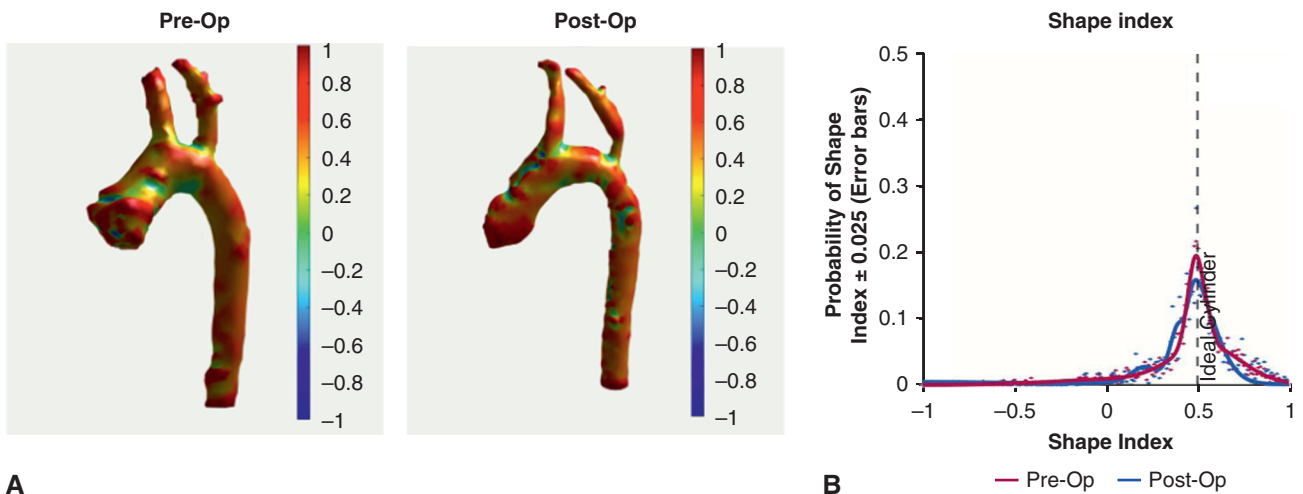
FIGURE 4. Shape index. A, Heatmap showing preoperative (*preop*) and postoperative (*postop*) shape index of porcine followed-up for 3 months. B, Preop and postop shape index distribution of porcine subjects after 3 months of follow-up. Preop and postop distributions are generally consistent.
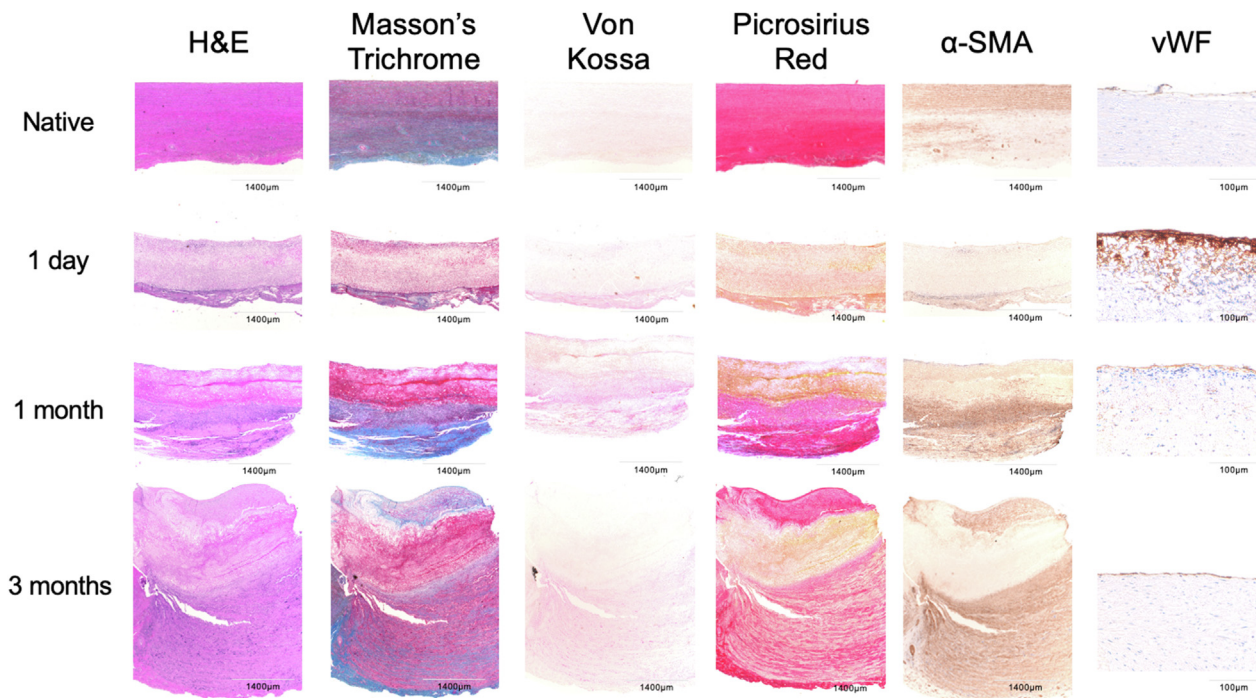
FIGURE 5. Compilation of all histological analyses performed on the native tissue, the explanted 1-day 3-dimensional tissue-engineered vascular graft (*3D TEVG*), 1-month 3D TEVG, and 3-month 3D TEVG. Histological staining included hematoxylin and eosin (*H&E*), Masson's trichrome, α-smooth muscle actin (*SMA*), Von Kossa, picrosirius red, and von Willebrand factor (*vWF*). These data support that 3D TEVG shows a single layer of endothelial cells, an organized smooth muscle cell layer, progressive extracellular matrix formation, and no ectopic calcification over time.

The mean change in 3D TEVG inner diameter was 2.02 ± 0.70 mm in the 1-day group, 2.79 ± 0 mm in the 1-month group, and 2.97 ± 2.52 mm in the 3-month group ($P = .7215$) (Figure 3).

Pre- and postoperative shape index data were quite similar; even 3 months after surgery, the TEVG exhibited symmetrical growth that was proportional to the growth of the native aorta (Figure 4).

4D Flow Analysis

CFD simulations helped design 3D TEVG with more optimal hemodynamics, with an emphasis on WSS and flow splits. During follow-up periods, only surviving animals (n = 8, PCL/PLCL only) underwent postoperative 4D flow MRI imaging. One subject who was followed-up at 1 month was excluded due to technical difficulties with postoperative MRI imaging.

The peak WSS of 3D TEVG was 24.50 ± 12.39 Pa at 1 day, 14.55 ± 0 Pa at 1 month, and 27.41 ± 21.52 Pa at 3 months, with no obvious deterioration of peak WSS over time ($P = .7933$). The peak energy loss of 3D TEVG was 1.19 ± 0.95 mW for 1 day, 0.87 ± 0 mW for 1 month, and 2.41 ± 1.15 mW for 3 months, with no apparent worsening of average energy loss over time ($P = .2571$). The right-handed helicity of 3D TEVG

was $2.10 \times 10^{-4} \pm 1.39 \times 10^{-4}$ Pa at 1 day, $1.32 \times 10^{-4} \pm 0$ Pa at 1 month, and $9.55 \times 10^{-4} \pm 7.60 \times 10^{-4}$ Pa at 3 months ($P = .1873$). The peak vorticity of the 3D TEVG was 123.93 ± 68.76 Pa at 1 day, 90.29 ± 0 Pa at 1 month, and 248.36 ± 157.60 Pa at 3 months ($P = .3660$) (Figure E3).

Histological Analysis

Biocompatibility of the graft, including patency and tissue degradation, was evaluated after the follow-up period. 3D TEVG histology showed a single layer of endothelial cells by hematoxylin and eosin, Masson's trichrome, picrosirius red, α-smooth muscle actin, and von Willebrand factor (vWF) antibody staining, an organized smooth muscle cell layer, and collagen deposition (Figure 5). Masson's trichrome staining and picrosirius red staining showed progressive extracellular matrix formation in the artificial vessels compared with native tissue; Von Kossa staining showed no ectopic calcification.

One day after graft implantation, strong positive vWF antibody staining indicated collagen and platelet adhesion to the graft during the acute phase. However, after 1 month, positive vWF staining confirmed the completion of endothelialization on the graft's internal surface. There was no graft-related stenosis, dilation, or rupture during the study
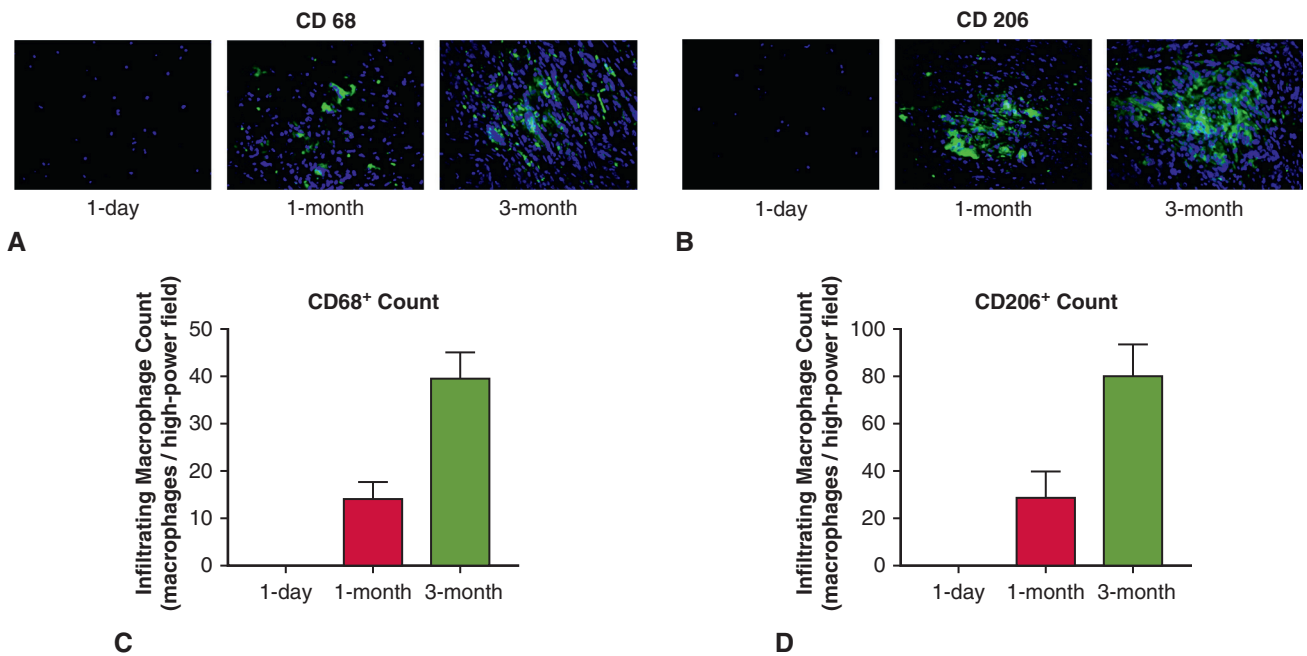
FIGURE 6. Macrophage analysis. A, CD68 antibody immunofluorescence stained images (40×) of tissue-engineered vascular graft (*TEVG*) at 1-day, 1-month, and 3-month follow-up. B, CD206 antibody immunofluorescence stained images (40×) of TEVG at 1-day, 1-month, and 3-month follow-up. C, Comparison of the number of CD68 antibody-positive macrophages in high-power field of TEVG at 1-day, 1-month, and 3-month follow-up. D, Comparison of the number of CD206 antibody-positive macrophages in high-power field of TEVG at 1-day, 1-month, and 3-month follow-up. Both CD68 and CD206 antibody-positive macrophages increased over time.

period, and no thrombus formation was observed either macroscopically or microscopically.

Other parameters investigated during histological analysis included vessel wall thickness and neointima thickness. The mean vessel wall thickness was 1569.73 ± 488.50 μm for native aorta, but increased between 1 and 3 months, with 1063.95 ± 221.71 μm at 1 day, 1467.57 ± 97.56 μm at 1 month, and 3448.09 ± 1275.17 μm at 3 months ($P < .0001$). On the other hand, the average neointima thickness was 26.48 ± 15.57 μm for native aorta, but increased

from relatively early on, with 27.4 ± 17.32 μm at 1 day, 914.55 ± 311.06 μm at 1 month, and 1050.95 ± 582.80 μm at 3 months for 3D TEVG ($P < .0001$) (Figure E4).

Graft degradation was detected by the presence of residual scaffold area by polarized light microscopy. The average value of residual scaffold in the 3D TEVG was $100\% \pm 0\%$ for 1 day, $62.87\% \pm 5.72\%$ for 1 month, and $40.46\% \pm 11.47\%$ for 3 months, indicating that graft degradation was gradual ($P = .0010$) (Figure E4). The number of CD 68+ and CD 206+ macrophages around the 3D
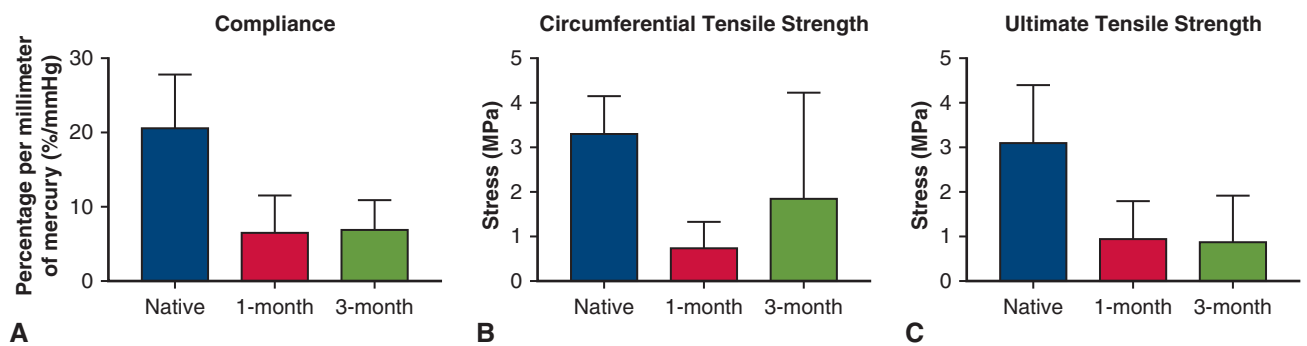
FIGURE 7. Mechanical analysis for native tissue, tissue-engineered vascular graft (*TEVG*) at 1-month, and TEVG at 3-month follow-up. A, compliance data. B, Circumferential tensile strength. C, Ultimate tensile strength data. After 3 months, the trend of tolerance remained the same as after 1 month.
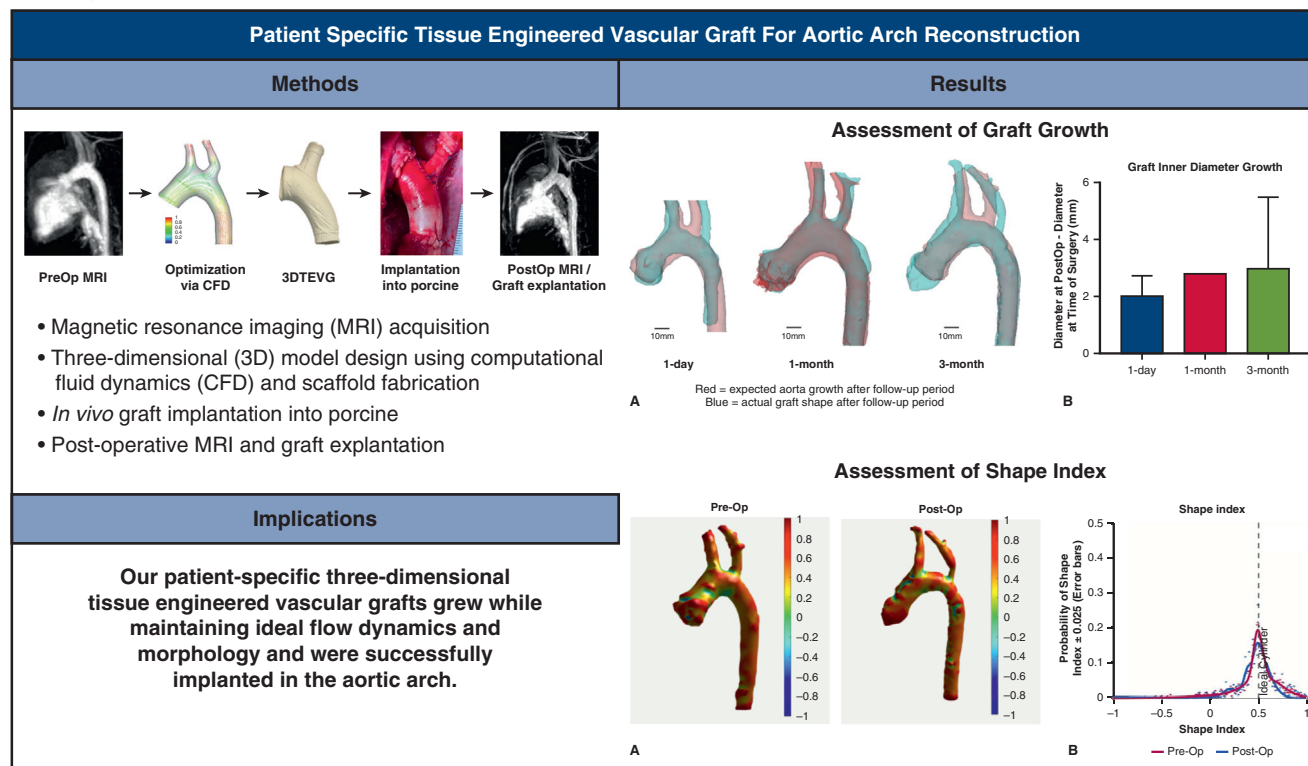
FIGURE 8. Graphical abstract. Patient-specific tissue-engineered vascular graft for aortic arch reconstruction. Assessment of Graft Growth. A, Overlay of pre- and post-operative MRI images. B, Comparison of mean graft inner diameter of each group using MRI images. The internal diameter increased, indicating graft growth. Assessment of Shape Index. A, Heatmap showing pre-operative and post-operative shape index of porcine followed up for 3 months. B, Pre- and post-operative distributions of shape index are generally consistent. *MRI*, Magnetic resonance imaging; *3D*, 3-dimensional; *CFD*, computational fluid dynamics.

TEVG continued to increase for three months ($P < .0001$) (Figure 6), inferring that the inflammatory process of vascular remodeling was sustained at the 3-month time point.

Mechanical Analysis

Finally, mechanical testing was performed to compare the compliance and strength of native tissue versus the PCL/PLCL 3D TEVG harvested grafts. Native tissue compliance was the highest at $20.61\% \pm 7.23\%$/mm Hg, whereas 3D TEVG compliance was lower at $6.46\% \pm 5.08\%$/mm Hg and $6.86\% \pm 4.02\%$/mm Hg at 1 month and 3 months, respectively ($P = .0497$) (Figure 7).

A similar trend was observed for tensile strength, with the highest circumferential and ultimate tensile strengths of 3.31 ± 0.85 MPa and 3.10 ± 1.30 MPa, respectively, for the native tissue. On the other hand, the circumferential and ultimate tensile strengths of 1-month 3D TEVGs were 0.74 ± 0.59 MPa and 0.94 ± 0.85 MPa, respectively. The circumferential and ultimate tensile strengths of the 3-month 3D TEVGs were 1.85 ± 2.39 MPa ($P = .0999$) and 0.86 ± 1.06 MPa ($P = .0874$) (Figure 7). Overall, the mechanical properties of the 3D TEVGs are somewhat different when compared with the native tissue results, but this is presumably due to the remodeling process.

DISCUSSION

The results of this study provide proof of concept of patient-specific 3D TEVG implantation in vivo in a porcine model and suggest which graft materials should be used. The 2 animals with PGA/PLCL implanted grafts died due to graft rupture, whereas all 8 pigs with PCL/PLCL grafts survived their respective scheduled follow-up periods without signs of graft rupture, dilation, or stenosis.

Among the unique features of a 3D TEVG is its ability to accommodate growth, which is not possible with

conventional grafts that are currently used in pediatric patients. The animal models exhibited growth in accordance with the general growth curve of their breed, gaining an average of 8.2 kg and 35.05 kg in weight at 1 and 3 months after surgery, respectively. During this time, the vasculature grew naturally in size, as evidenced by an increase in the inner diameter of the native aortic tissue. The internal diameter of the 3D TEVG also increased, indicating graft growth. The graft maintained a good shape index and did not experience abnormal WSS, energy loss, helicity, or vorticity over time, evidence that it adapted to the natural curvature of the aorta and maintained appropriate hemodynamics.

Only the animals with 1:1 PCL/PLCL aortic grafts were able to survive the 3-month follow-up period. The average value of residual scaffold in the PCL/PLCL graft was $40.46\% \pm 11.47\%$ after the 3-month period. In a previous study of 1:1 PGA/PLCL TEVGs implanted in porcine pulmonary arteries, degradation progressed rapidly with an average residual scaffold area of $21.37\% \pm 20.46\%$ after 10 weeks.[16] Thus, premature degradation may be a risk for rupture and mass formation.

The histological analysis conducted in this study confirmed that the 3D TEVG was biocompatible and functioned similarly to native aortic vessels. Previous studies have reported limited cellular infiltration and integration of PCL/PLCL grafts implanted in arteries, with high rates of thrombosis and neointimal hyperplasia.[20,21] Intimal thickening and subsequent vascular remodeling over time can lead to stenosis and occlusion, which are associated with various health risks such as hypertension, myocardial infarction, and stroke.[22] However, this study showed that large-diameter grafts may not cause graft stenosis compared with small-diameter grafts, although there may be some intimal thickening. Qualitatively, the histological data showed a monolayer of endothelial cells, an organized smooth muscle cell layer, and collagen deposition. These findings are promising because endothelial or smooth muscle cell dysfunction is a characteristic feature of human diseases such as atherosclerosis[23] and sporadic venous vascular malformations.[24] The presence of collagen indicates an initial processing of neointimal tissue formation and remodeling, which may have contributed to the adequate resistance seen in mechanical testing.

Our previous research has shown that a scaffold seeded with bone marrow mononuclear cells can transform into a living vascular conduit capable of growing, repairing, and remodeling via an inflammation-mediated process.[25] In this study, the number of CD 68+ and CD 206+ macrophages around the 3D TEVGs continued to increase over a 3-month period, inferring that inflammation due to vascular remodeling was underway. However, excessive macrophage infiltration can contribute to occlusive vascular

neotissue hyperplasia, as suggested by our previous studies.[26,27] Therefore, further long-term follow-up is needed to determine how the inflammatory process proceeds.

The result of compliance discrepancy between the native tissue versus TEVG could also be explained by the remodeling process of TEVG. We envision that TEVG will be implanted in children in the future, but there are no studies that directly compare the compliance of a 27-week-old porcine subject's aorta used in this study with that of children. It has been reported that porcine aortas are more flexible than those of older humans,[28] but young human aortas may be more compliant because of their greater tissue elasticity. Thus, it is critical to investigate the mechanical properties of TEVGs in longer-term studies to evaluate its remodeling process.

Among the goals of 3D TEVGs is to improve hemodynamic performance in addition to growth accommodation. WSS can be influenced by various factors, but elevated WSS levels can change the behavior of endothelial cells, leading to inflammation[29] and potentially causing thrombosis formation.[30] Abnormal WSS has also been linked to high-risk plaque development and rupture, which can result in atherosclerosis and myocardial infarction.[31] To optimize the hemodynamic performance of the 3D TEVGs, minimizing WSS was a key goal of our CFD simulations when designing the graft shape. We found that the average WSS remained generally stable, and there were no anomalies in other hemodynamic parameters such as energy loss, helicity, or vorticity. This suggests that grafts created using CFD analysis could maintain ideal hemodynamics even after 3 months due to graft growth.

Although 3D TEVGs showed promising results in replacing the aorta and preserving its morphology in 3 months, this proof of concept study has several limitations. First, the small sample size consists of only 2 pig models with PGA/PLCL and 8 pig models with PCL/PLCL, which reduces statistical power and restricts the ability to generalize the results to a broader population. Another challenge is achieving proper integration of the TEVG with the surrounding tissue, which may be critical to the long-term success of the graft and future growth. The 3D TEVG component at the 3-month follow-up of this study was generally still in place; however, longer-term data on its safety and efficacy are still needed. In particular, the morphology and hemodynamics after proper integration with autologous tissue should be evaluated in the future to understand graft patency, resistance to wear and tear, and the body's long-term biological response.

Precise implantation location is a critical factor in achieving optimal 3D TEVGs. Obtaining accurate 3D orientation during surgery is challenging, leading to deviations from surgical CFD simulations. Our previous research

in porcine models found that greater displacement during surgical implantation resulted in higher WSS levels despite efforts to optimize WSS.[18] Another study found that deviations in predicted flow distributions in Fontan conduits also occurred due to offset errors during implantation.[32] To ensure accuracy during cardiac implantation procedures, future work must focus on mitigating this confounding variable. Creating a tool that ensures precision could be a solution, such as augmented reality and holograms as surgical planning tools for CHD to improve the understanding of complex morphology.[33,34]

CONCLUSIONS

Overall, our patient-specific 3D TEVGs made by a 1:1 PCL/PLCL blend were successfully implanted into the descending aorta from the aortic arch in 8 porcine models (Figure 8). The grafts did not present stenosis or aortic aneurysm formation and were able to accommodate porcine growth, illustrate optimal anatomic conformity, and maintain ideal flow dynamics over 3 months. This proof of concept study demonstrates the potential of patient-specific 3D TEVGs in the aortic arch for descending aorta reconstruction, warranting further longer-term studies.

Conflict of Interest Statement

Drs Johnson, Krieger, and Hibino are inventors listed on international patent WO/2017/035500Al (Patient-Specific Tissue Engineered Vascular Graft Utilizing Electrospinning). Dr Johnson is an equity holder in Nanofiber Solutions. All other authors reported no conflicts of interest.

The *Journal* policy requires editors and reviewers to disclose conflicts of interest and to decline handling manuscripts for which they may have a conflict of interest. The editors and reviewers of this article have no conflicts of interest.

References

1. van der Linde D, Konings EE, Slager MA, et al. Birth prevalence of congenital heart disease worldwide: a systematic review and meta-analysis. *J Am Coll Cardiol*. 2011;58(21):2241-2247.
2. Spector LG, Menk JS, Knight JH, et al. Trends in long-term mortality after congenital heart surgery. *J Am Coll Cardiol*. 2018;71:2434-2446.
3. Jacobs ML, Jacobs JP, Hill KD, et al. The society of thoracic surgeons congenital heart surgery database: 2019 update on research. *Ann Thorac Surg*. 2019;108: 671-679.
4. van der Slegt J, Steunenberg SL, Donker JM, et al. The current position of precuffed expanded polytetrafluoroethylene bypass grafts in peripheral vascular surgery. *J Vasc Surg*. 2014;60:120-128.
5. Iguidbashian J, Feng Z, Colborn KL, et al. Open chest duration following congenital cardiac surgery increases risk for surgical site infection. *Pediatr Cardiol*. 2022;30.
6. Holst KA, Dearani JA, Burkhart HM, et al. Risk factors and early outcomes of multiple reoperations in adults with congenital heart disease. *Ann Thorac Surg*. 2011;92(1):122-128; discussion 129-130.
7. Mascio CE, Pasquali SK, Jacobs JP, Jacobs ML, Austin EH III. Outcomes in adult congenital heart surgery: analysis of the Society of Thoracic Surgeons database. *J Thorac Cardiovasc Surg*. 2011;142:1090-1097.
8. Hibino N, Duncan DR, Nalbandian A, et al. Evaluation of the use of an induced puripotent stem cell sheet for the construction of tissue-engineered vascular grafts. *J Thorac Cardiovasc Surg*. 2012;143(3):696-703.
9. Shinoka T, Breuer C. Tissue-engineered blood vessels in pediatric cardiac surgery. *Yale J Biol Med*. 2008;81(4):161-166.
10. Aslan S, Halperin H, Olivieri L, et al. Design and simulation of patient-specific tissue-engineered bifurcated right ventricle-pulmonary artery grafts using computational fluid dynamics. In: 2019 IEEE 19th International Conference on Bioinformatics and Bioengineering (BIBE), Athens, Greece. 2019:1012-1018.
11. Liu X, Aslan S, Hess R, et al. Automatic shape optimization of patient-specific tissue engineered vascular grafts for aortic coarctation. *Annu Int Conf IEEE Eng Med Biol Soc*. 2020;2020:2319-2323.
12. Liu X, Aslan S, Kim B, et al. Computational Fontan analysis: preserving accuracy while expediting workflow. *World J Pediatr Congenit Heart Surg*. 2022; 13(3):293-301.
13. Miyaji K, Miyazaki S, Itatani K, Oka N, Kitamura T, Horai T. Novel surgical strategy for complicated pulmonary stenosis using haemodynamic analysis based on a virtual operation with numerical flow analysis. *Interact Cardiovasc Thorac Surg*. 2019;28(5):775-782.
14. Fukunishi T, Best CA, Sugiura T, et al. Preclinical study of patient-specific cell-free nanofiber tissue-engineered vascular grafts using 3-dimensional printing in a sheep model. *J Thorac Cardiovasc Surg*. 2017;153(4):924-932.
15. Yeung E, Inoue T, Matsushita H, et al. In vivo implantation of 3-dimensional printed customized branched tissue engineered vascular graft in a porcine model. *J Thorac Cardiovasc Surg*. 2020;159(5):1971-1981.e1.
16. Hayashi H, Contento J, Matsushita H, et al. Validity of customized branched tissue engineered vascular graft in a porcine model. *Ann Thorac Surg Short Rep*. 2023;1(3):426-430.
17. Contento J, Mass P, Cleveland V, et al. Location matters: offset in tissue-engineered vascular graft implantation location affects wall shear stress in porcine models. *J Thorac Cardiovasc Surg Open*. 2022;12:355-363.
18. Barker AJ, van Ooij P, Bandi K, et al. Viscous energy loss in the presence of abnormal aortic flow: energy loss in the presence of abnormal aortic flow. *Magn Reson Med*. 2014;72:620-628.
19. Koenderink JJ, van Doorn AJ. Surface shape and curvature scales. *Image Vis Comput*. 1992;10(8):557-564.
20. Rodríguez-Soto MA, Polanía-Sandoval CA, Aragón-Rivera AM, et al. Small diameter cell-free tissue-engineered vascular grafts: biomaterials and manufacture techniques to reach suitable mechanical properties. *Polymers*. 2022; 14(17):3440.
21. Fayon A, Menu P, El Omar R. Cellularized small-caliber tissue-engineered vascular grafts: looking for the ultimate gold standard. *NPJ Regen Med*. 2021;6(1):46.
22. Morii C, Tanaka HY, Izushi Y, et al. 3D in vitro model of vascular medial thickening in pulmonary arterial hypertension. *Front Bioeng Biotechnol*. 2020;8:482.
23. Rajendran P, Rengarajan T, Thangavel J, et al. The vascular endothelium and human diseases. *Int J Biol Sci*. 2013;9:1057-1069.
24. Chen G, Ren JG, Zhang W, et al. Disorganized vascular structures in sporadic venous malformations: a possible correlation with balancing effect between Tie2 and TGF-β. *Sci Rep*. 2014;4:5457.
25. Roh JD, Sawh-Martinez R, Brennan MP, et al. Tissue-engineered vascular grafts transform into mature blood vessels via an inflammation-mediated process of vascular remodeling. *Proc Natl Acad Sci U S A*. 2010;107:4669-4674.
26. Hibino N, Villalona G, Pietris N, et al. Tissue-engineered vascular grafts form neovessels that arise from regeneration of the adjacent blood vessel. *FASEB J*. 2011;25(8):2731-2739.
27. Hibino N, Mejias D, Pietris N, et al. The innate immune system contributes to tissue-engineered vascular graft performance. *FASEB J*. 2015;29(6):2431-2438.
28. Li K, Wang Q, Pham T, Sun W. Quantification of structural compliance of aged human and porcine aortic root tissues. *J Biomed Mater Res*. 2014;102(7): 2365-2374.
29. Hathcock JJ. Flow effects on coagulation and thrombosis. *Arterioscler Thromb Vasc Biol*. 2006;26:1729-1737.
30. Boumpouli M, Sauvage EL, Capelli C, Schievano S, Kazakidi A. Characterization of flow dynamics in the pulmonary bifurcation of patients with repaired tetralogy of Fallot: a computational approach. *Front Cardiovasc Med*. 2021;8:703-717.

31. Eshtehardi P, Brown AJ, Bhargava A, et al. High wall shear stress and high-risk plaque: an emerging concept. *Int J Cardiovasc Imaging*. 2017;33:1089-1099.
32. Trusty PM, Wei ZA, Slesnick TC, et al. The first cohort of prospective Fontan surgical planning patients with follow-up data: how accurate is surgical planning? *J Thorac Cardiovasc Surg*. 2019;157(3):1146-1155.
33. Munawar A, Li Z, Kunjam P, et al. Virtual reality for synergistic surgical training and data generation. *Computer Methods Biomechanics Biomedical Engineer Imaging Visualization*. 2022;10(4):366-374.
34. Brun H, Bugge RAB, Suther LKR, et al. Mixed reality holograms for heart surgery planning: first user experience in congenital heart disease. *Eur Heart J Cardiovasc Imaging*. 2019;20(8):883-888.
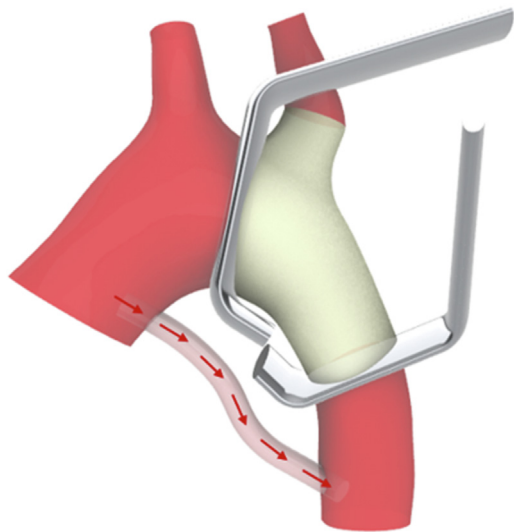
FIGURE E1. After partial bypass of the ascending and descending aorta, the distal aortic arch to the proximal descending aorta, including the left subclavian artery bifurcation, was resected and a 3-dimensional tissue-engineered vascular graft was implanted. The *red arrows* indicate that the partial bypass preserves circulation in the lower body.
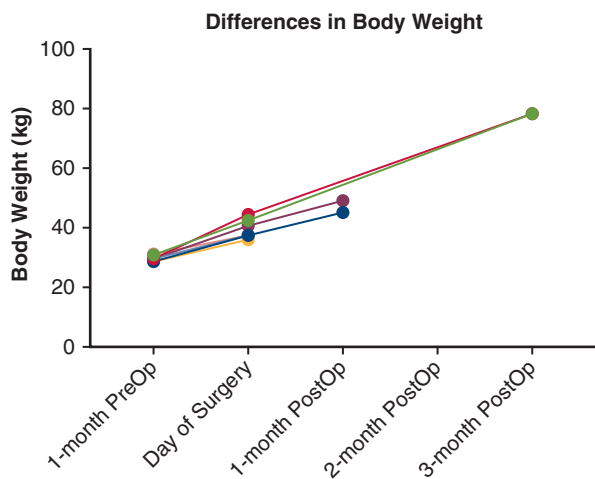
FIGURE E2. Differences in body weight over the porcine life span. Body weight data were collected 4 weeks before surgery (preop), at the time of surgery, and on the last day of follow-up (postop). *preop*, Preoperative; *postop*, postoperative.
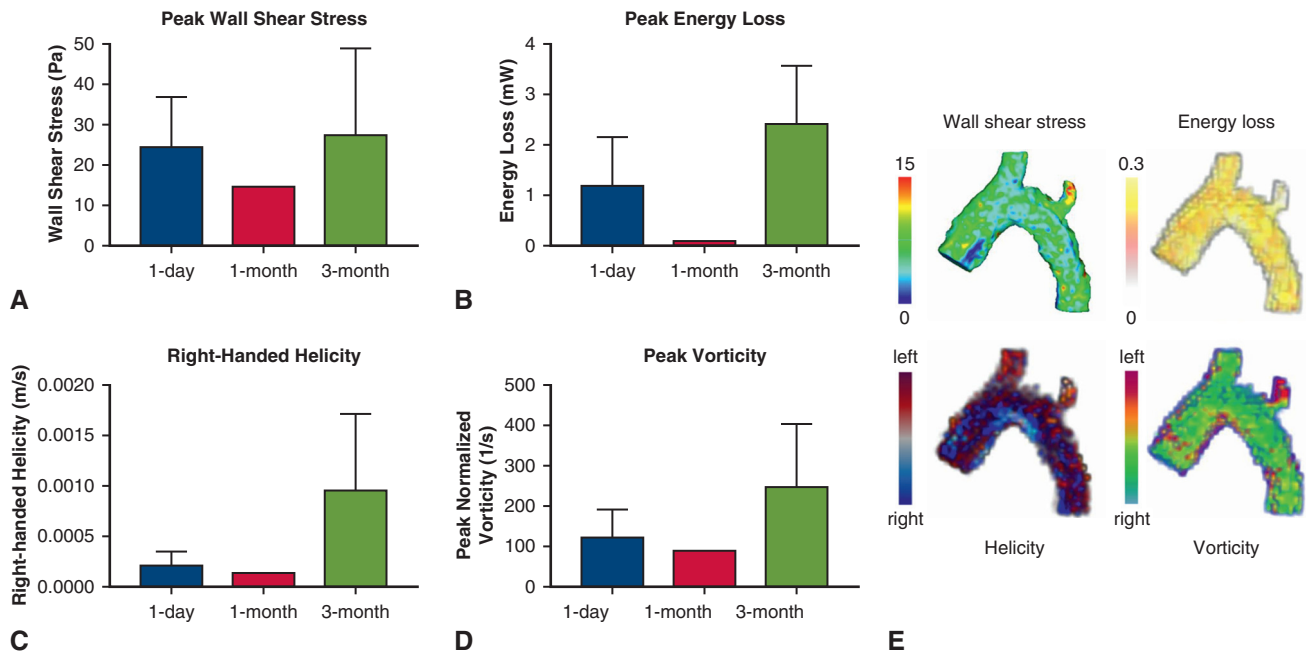
FIGURE E3. Magnetic resonance imaging (*MRI*) 4-dimensional flow data of the 3-dimensional tissue-engineered vascular graft at 1 day, 1 month, and 3 months after surgery. A, Peak wall shear stress (*WSS*). B, Peak energy loss. C, Helicity. D, Peak vorticity. There were no anomalies in the peak WSS, peak energy loss, helicity, or peak vorticity. E, Heat map of WSS, energy loss, helicity, or vorticity.
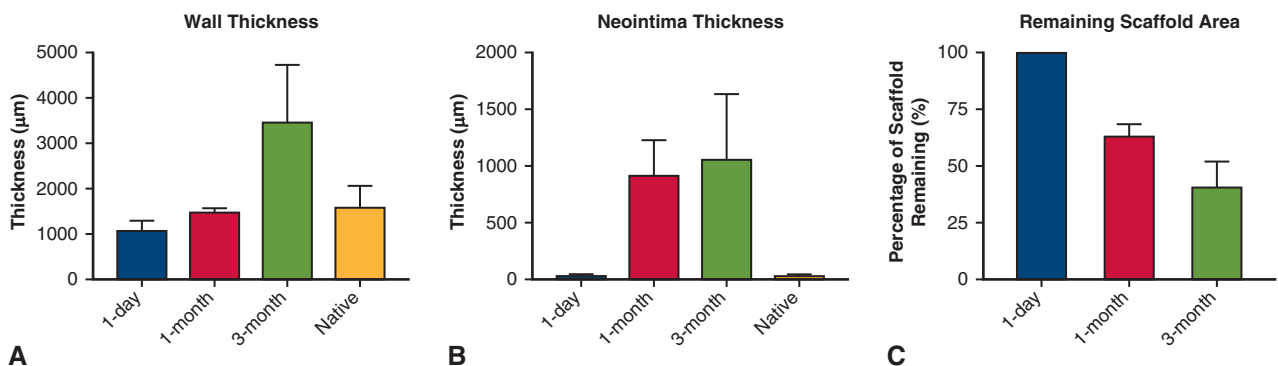
FIGURE E4. A, Histological analysis of wall thickness for 3-dimensional tissue-engineered vascular graft (*3D TEVG*) at 1 day, 1 month, and 3 months, and the native tissue at 3 months after surgery. B, Histological analysis of intima thickness for 3D TEVG at 1 day, 1 month, and 3 months, and the native tissue at 3 months after surgery. After 3 months, both wall thickness and intima thickness show thickening. C, Percentage of remaining scaffold area over time. A gradual decrease in graft components is observed.